Journal of Applied Physics

RESEARCH ARTICLE | MARCH 12 2025

Direct measurement of lattice behavior during femtosecond laser-driven shock front formation in copper

Naoya Egashira (江頭 尚弥); Tomoki Matsuda (松田 朋己); Takuo Okuchi (奥地 拓生); Yusuke Seto (瀬戸 雄介); Yusuke Ito (伊藤 佑介); Takahisa Shobu (菖蒲 敬久); Nobuhiko Nakanii (中新 信彦); Yuichi Inubushi (犬伏 雄一); Tadashi Togashi (富樫 格); Kohei Miyanishi (宮西 宏併); Tsutomu Mashimo (真下 茂); Tomokazu Sano (佐野 智一)

J. Appl. Phys. 137, 105903 (2025)
https://doi.org/10.1063/5.0253150

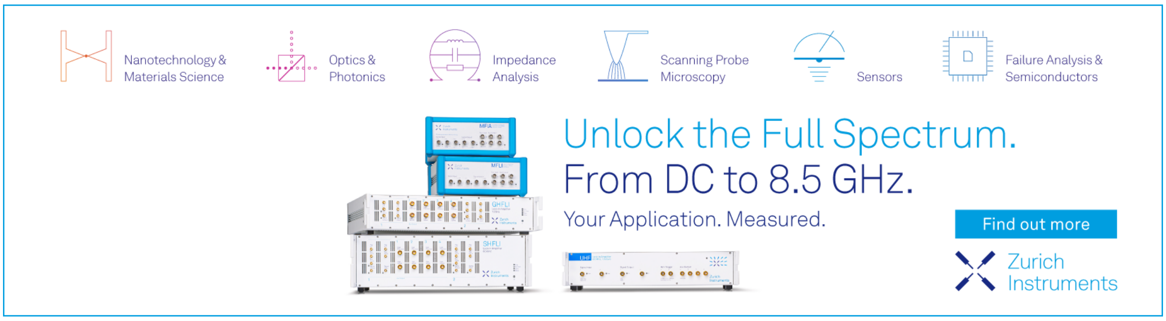

AIP Publishing

Journal of Applied Physics | ARTICLE | pubs.aip.org/aip/jap

Direct measurement of lattice behavior during femtosecond laser-driven shock front formation in copper

Cite as: J. Appl. Phys. **137**, 105903 (2025); doi: 10.1063/5.0253150
Submitted: 15 December 2024 · Accepted: 18 February 2025 ·
Published Online: 12 March 2025

View Online Export Citation CrossMark

Naoya Egashira (江頭 尚弥),[1] Tomoki Matsuda (松田 朋己),[1] Takuo Okuchi (奥地 拓生),[2] Yusuke Seto (瀬戸 雄介),[3] Yusuke Ito (伊藤 佑介),[4] Takahisa Shobu (菖蒲 敬久),[5] Nobuhiko Nakanii (中新 信彦),[6] Yuichi Inubushi (犬伏 雄一),[7,8] Tadashi Togashi (富樫 格),[7,8] Kohei Miyanishi (宮西 宏併),[8] Tsutomu Mashimo (真下 茂),[9] and Tomokazu Sano (佐野 智一)[1,a)]

AFFILIATIONS

[1]Division of Materials and Manufacturing Science, Graduate School of Engineering, Osaka University, Suita, Osaka 565-0871, Japan
[2]Division of Quantum Beam Material Science, Institute for Integrated Radiation and Nuclear Science, Kyoto University, Kumatori, Osaka 590-0494, Japan
[3]Department of Geosciences, Graduate School of Science, Osaka Metropolitan University, Osaka 558-8585, Japan
[4]Department of Mechanical Engineering, School of Engineering, The University of Tokyo, Bunkyo, Tokyo 113-8656, Japan
[5]Sector of Nuclear Science Research, Japan Atomic Energy Agency, Sayo, Hyogo 679-5148, Japan
[6]Kansai Institute for Photon Science (KPSI), National Institutes for Quantum Science and Technology (QST), Kizugawa, Kyoto 619-0215, Japan
[7]Japan Synchrotron Radiation Research Institute, Sayo, Hyogo 679-5198, Japan
[8]RIKEN SPring-8 Center, Sayo, Hyogo 679-5148, Japan
[9]Faculty of Advanced Science and Technology, Kumamoto University, Kumamoto 860-8555, Japan

[a)]**Author to whom correspondence should be addressed:** sano@mapse.eng.osaka-u.ac.jp. **Tel. & Fax:** +81-6-6879-7534

ABSTRACT

Femtosecond laser-driven shock waves exhibit characteristic features that form distinctive microstructures not formed by plate impacts or nanosecond laser-driven shock waves. A key to understanding this phenomenon is understanding the lattice behavior inside the shock front, which is the boundary between the ambient and shock compression states. However, direct measurements of the lattice spacing inside a femtosecond laser-driven shock front have not yet been performed. Here, we report *in situ* measurements of lattice spacing using x-ray free electron laser diffraction with a pulse width of <10 fs during the shock rise in single-crystal copper irradiated directly in air with a femtosecond laser pulse on the order of 10^{14} W/cm^2 at a pulse width of 101 fs. The lattice spacing of the femtosecond laser-irradiated single-crystal Cu (002) plane starts to compress 6.3 ps after femtosecond laser irradiation. It takes 15.7 ps for the plane to reach peak compression, at which point the compressive elastic strain is 24.3%. Therefore, the shock front was found to form at an elastic compressive strain rate of 1.55×10^{10}/s in this shock-driving situation. It is suggested that the initiation of plasticity under such ultrafast deformation at the most elastic compression is based on both dislocation multiplication and dislocation generation mechanisms.

I. INTRODUCTION

Femtosecond lasers[1] have been used for surface modification using shock effects as a new processing method[2] in recent years as well as for microfabrication owing to their ultrashort pulse widths.[3] When femtosecond laser pulses above a certain threshold intensity are directly irradiated onto the surface of a metallic material, shock waves are driven and propagate inside the metal. The femtosecond laser-driven shock wave causes the plastic deformation of the metal, which hardens the surface and induces compressive residual stress, resulting in longer fatigue life and higher corrosion resistance.[4–6] In the region where the femtosecond laser-driven shock wave propagates, characteristic microstructures, such as metastable[7–10] and unique dislocation structures,[11,12] are observed, which cannot be seen with conventional shock compression methods. Therefore, femtosecond laser-driven shock waves are predicted to have different characteristics from conventional shock waves.

Femtosecond laser-driven shock wave measurements were first performed by Evans *et al.*[13] They measured the ultrafast deformation behavior at an interface between a thin metal film deposited on a glass substrate and the glass immediately after femtosecond laser irradiation and reported that shock waves with amplitudes of 100–300 GPa were driven in the Hugoniot state. The ultrafast lattice behavior of iron directly irradiated by a femtosecond laser was analyzed using x-ray free electron laser (XFEL) diffraction by Sano *et al.*[14] After elastic compression for up to 50 ps after femtosecond laser irradiation, plastic deformation began, and elastic and plastic strains balanced over 100 ps, followed by a Hugoniot state for a few nanoseconds. These results suggest that the formation of unique microstructures in femtosecond laser-shocked materials is due to the shock wave rise. These are the only two reported *in situ* experimental measurements of the shock deformation behavior of metals directly irradiated with femtosecond lasers.

Previous studies, except those by Evans *et al.*[13] and Sano *et al.*,[14] have used a plasma confinement scheme, in which a pump laser beam passes through a glass substrate and irradiates a thin metal film deposited on the glass, while a probe laser irradiates the free surface of the metal film. The ultrafast behavior of materials using such a scheme has been experimentally diagnosed and well-studied using ultrafast pump–probe methods, such as ultrafast interferometry and dynamic ellipsometry.[15–17] A pioneering study on femtosecond laser-driven shock wave rise measurements was performed by Gahagan *et al.*[18] Femtosecond lasers with wavelengths of 400 or 800 nm, pulse widths of 130 fs, and pulse energies of 0.2–0.5 mJ were directed through glass coverslips onto the deposited polycrystalline Al and Ni thin films of 0.25–2 μm thickness. Shock wave velocities of ∼5 km/s corresponding to pressures of 3–5 GPa and 10%–90% rise times of < 6.25 ps were measured using frequency-domain interferometry with sub-picoseconds temporal resolution. Ashitkov *et al.* irradiated polycrystalline aluminum thin films through their glass substrates with femtosecond laser pulses with a pulse width of 150 fs and a fluence of 1.3 J/cm^2 and studied the driven shock wave using femtosecond interferometric microscopy.[19] The results did not show the expected splitting of the shock wave into elastic and plastic compressive waves, and only elastic shock waves of 9–13 GPa were measured based on the relationship between the shock wave velocity and the particle velocity behind the shock front. The shear stress achieved by this process was close to the ultimate value estimated for aluminum, and the spall strength determined at a tensile strain rate of 10^9/s was more than half of the ultimate strength of aluminum. The invariance of the dissipative action of the shock waves at very high strain rates, driven by clipped sub-nanosecond lasers irradiating thin metal films through glass substrates, was reported by Crowhurst *et al.*[20] The invariance of the Swegle and Grady fourth power scaling[21–23] and the dissipative action is maintained even at strain rates exceeding 10^{10}/s, corresponding to a peak stress of 43 GPa. In these schemes, the laser-irradiated metal surface is the interface with the glass substrate; therefore, electrons and ions ejected during or immediately after femtosecond laser irradiation are trapped at the interface. Therefore, there is a concern that electrons and ions ejected from the metal at the beginning of femtosecond laser irradiation may affect shock wave formation due to preheating and plasma expansion.[24–27] That is, the behavior of shock waves formed in a plasma-confined scheme may differ from that of shock waves driven by femtosecond laser irradiation with an unconfined metal surface.

All previous studies, except the XFEL diffraction measurements reported by Sano *et al.*,[14] measured the surface displacement velocities and estimated the particle velocities. Although this method can provide information on the hydrodynamic behavior of shock waves, the distinction and interpretation of elastic and plastic waves can be difficult when their behaviors are complicated.[19,28–30] A very large pressure gradient is formed inside the shock front, which has the potential to create new dislocations owing to the large deviatoric stresses.[31] Therefore, the key to understanding the phenomena of shock-induced elasto-plastic transitions in materials is to understand the behavior of the shock front. However, the lattice spacing inside the shock front has never been measured, although the behavior of the shock front, which is driven by a nanosecond laser pulse, has been imaged using the XFEL[32] and the laser-plasma x-ray source.[33,34] The objective of the present study is to measure the lattice spacings during shock front formation driven by the femtosecond laser irradiation of a metal surface; to the best of our knowledge, such measurements have not yet been reported in scientific literature studies. Because it has been reported that the rise time of a femtosecond laser shock wave in a plasma-confined scheme is within 10 ps,[18] a sub-picosecond temporal resolution is required, even for direct irradiation schemes. The femtosecond laser pump and XFEL diffraction measurements were performed at SPring-8 Angstrom Compact free electron LAser (SACLA) facility[35] using an XFEL with a pulse width of 10 fs as the probe. The elastic behavior of the shock wave during its rise can be determined by obtaining the temporal evolution of the lattice strain from the shift in the Bragg peak to the shock wave rise.

II. METHODS

Copper was chosen as the target material in this study because it is suitable for shock-rise characterization owing to the absence of phase transitions at relatively low pressures and its well-studied shock compression properties.[36–38] A (001) copper single crystal with a purity of 99.9999% (MaTecK, 70× 3 mm^2, 2 mm thickness) was used. The femtosecond laser pump–XFEL probe experiment was performed in experimental hatch EH2 at beamline BL3 of the SACLA facility. Figure 1 shows a schematic of the experimental setup.

The angle between the femtosecond laser beam for the pump and the XFEL beam for the probe was nearly perpendicular, and the pump laser irradiated the sample surface tilted by an angle of ω° with respect to the XFEL beam. The XFEL beam was irradiated with a time delay t at the location where the pump laser irradiated the sample. The XFEL beams scattered and diffracted at the sample surface were obtained using a two-dimensional detector. The pump laser was a

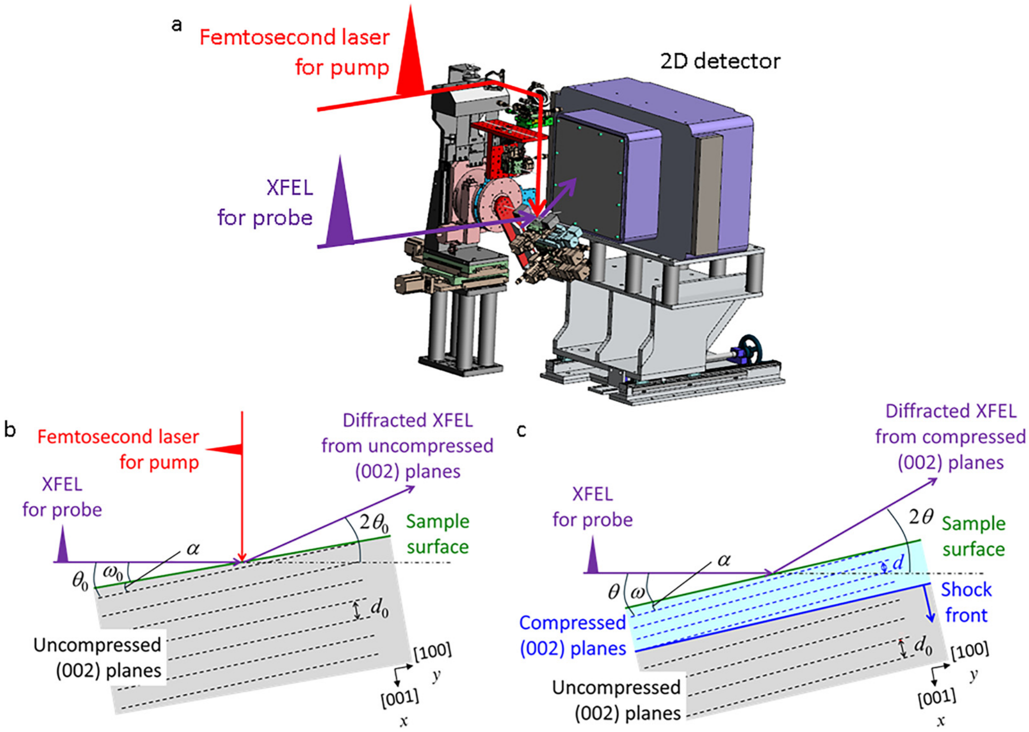

FIG. 1. Schematic illustration of the experimental setup comprising the femtosecond laser pump and XFEL diffraction systems. (a) The femtosecond laser pump and XFEL probe beams are nearly perpendicular; the pump laser is irradiated on the sample surface tilted by $\omega°$ with respect to the XFEL beam. The XFEL beam scattered and diffracted at the sample surface is received using a two-dimensional detector. (b) Situation before the femtosecond laser pulse irradiation onto the material. When the Bragg angle for the initial uncompressed (002) plane spacing d_0 is θ_0 and the angle between the XFEL beam and the sample surface at this time is ω_0, $\theta_0 = \omega_0 + \alpha$. (c) Situation after the femtosecond laser pulse irradiation onto the material. At $t = 0$, a femtosecond laser beam irradiates the sample surface, forming a shock wave parallel to the sample surface, i.e., nearly parallel to the (002) plane, which propagates in the [001] direction. When the (002) plane is elastically compressed by ε (%) due to the femtosecond laser-driven shock compression at t, the lattice spacing of the compressed (002) plane becomes $d = (100 - \varepsilon)d_0/100$. When the Bragg angle with respect to d is θ, $\theta = \sin^{-1}[100 \sin \theta_0/(100 - \varepsilon)]$. The angle between the XFEL beam and the sample surface at this time is $\omega = \theta - \alpha$.

femtosecond laser with a central wavelength of 797 nm with a bandwidth of 23.5 nm [full width at half maximum (FWHM)], a pulse width of 101 fs (FWHM), and a pulse energy of 10.7 mJ.

As shown in Fig. 1(a), a Cu (001) surface was irradiated with a femtosecond laser beam focused by a plano–convex lens with a focal length of 150 mm. The diameter of the crater formed by the femtosecond laser irradiation was approximately 150 μm, corresponding to an average intensity of 6.0×10^{14} W/cm^2 and an average fluence of 61 J/cm^2 at the sample surface. An XFEL pulse with a monochromated photon energy of 13 keV with an energy spread of 0.01% and a pulse width of <10 fs was used as the probe beam.[39] The XFEL pulse was focused to a diameter of about 100 μm on the sample surface using a Be lens. The spatial overlap between the pump and probe lasers was ensured using a GAFCHROMIC film that fluoresced for both the pump and probe lasers. A high-speed photodiode was used to adjust the delay time to zero such that the timing of the XFEL signal coincided with the increase in the femtosecond laser pulse signal. The XFEL and pump laser pulses were synchronized in time with a shot-to-shot fluctuation in the sub-picosecond range. The delay time t of the XFEL pulse from the femtosecond laser pulse was varied using an electrical delay system. A two-dimensional detector (Rayonix MX300-HS) with a pixel size of $78 \times 78\,\mu$m^2 was positioned nearly perpendicular to the XFEL beam and at a distance of approximately 130 mm to the sample. Geometric parameters, such as the actual distance between the laser-irradiated spot and the detector, and the tilt angle of the detector, were calibrated using CeO_2 powders as a standard material and the IPAnalyzer software.[40,41]

The lattice spacing of the (002) plane was measured, which was nearly parallel to the sample surface as shown in Fig. 1(b). Although the sample surface was a (002) plane, there was a slight misalignment angle of α degrees between the sample surface and the (002) plane. When the Bragg angle for the initial uncompressed (002) plane spacing d_0 is θ_0, the misalignment angle between the sample surface and the (002) plane is α, and the angle between the XFEL beam and the sample surface is ω_0, so $\theta_0 = \omega_0 + \alpha$. At $t = 0$ s, a femtosecond laser beam is irradiated onto the sample surface, driving a shock wave on the sample surface. The shock front is formed parallel to the sample surface, i.e., nearly parallel to the (002) plane, and propagated in the [001]

TABLE I. Femtosecond laser pump and XFEL diffraction measurement conditions for single-crystal copper.

Elastic compressive strain ε (%)	Tilt angle ω (°)	Bragg angle 2θ (°)	X-ray penetration depth (μm)
5	15.20	32.28	1.3
15	17.04	36.21	1.5
25	19.39	41.24	1.7
30	20.84	44.34	1.8

direction. As shown in Fig. 1(c), when the (002) plane is elastically compressed by ε (%) due to the femtosecond laser-driven shock compression at t, the lattice spacing of the compressed (002) plane becomes $d = (100 - \varepsilon)d_0/100$. When the Bragg angle with respect to d is θ, $\theta = \sin^{-1}[100 \sin \theta_0/(100 - \varepsilon)]$. In this case, ω becomes $\omega = \theta - \alpha = \sin^{-1}[100 \sin \theta_0/(100 - \varepsilon)] - \alpha$. In other words, by changing ω, the Bragg peak corresponding to d, that is elastically compressed by ε (%), can be detected. The lattice spacing of the copper single crystal used for the measurement was measured to be $d_0 = 1.80545$ Å at $\omega_0 = 14.42°$ and $2\theta_0 = = 30.6298°$, giving $\alpha = 0.8949°$. Based on these values, the ω values, at which elastically compressed strains of approximately 5, 15, 25, and 30% were detected, were calculated. ω used in the measurement, corresponding diffraction angle 2θ, strain, and x-ray penetration depth (i.e., the measurement area in the depth direction) are listed in Table I. t was varied in steps of 2 ps, and the corresponding ε and changes in d were evaluated.

III. RESULTS

Figures 2(a)–2(d) show the typical diffraction patterns recorded at different t and ω values. The vertical direction in the figure represents the angle in the 2θ direction. Figure 2(a) shows the unperturbed pattern recorded before the pump laser irradiation at $\omega = 14.42°$. A Bragg spot reflected from the (002) plane was observed at $2\theta_0 = 30.6298°$. Figures 2(b)–2(d) show the data acquired at $\omega = 15.20°$ at $t = 14$ ps, $\omega = 17.04°$ at $t = 20$ ps, and $\omega = 19.39°$ at $t = 26$ ps, corresponding to approximate ε values of 5%, 15%, and 25%, respectively. In all cases, Bragg spots were observed at higher angles than the uncompressed (002) spots. No Bragg spots were observed at $\omega = 20.84°$, corresponding to $\varepsilon \approx 30\%$.

Figure 3 shows one-dimensional (1D) profiles converted from three-dimensional (3D) images, as shown in Fig. 2, using IPAnalyzer software.[40,41] Figure 3(a) shows the 1D profile in the uncompressed state, shown in Fig. 2(a). Figures 3(b)–3(d) show the 1D profiles at $\omega = 15.20°$ ($\varepsilon \approx 5\%$), $\omega = 17.04°$ ($\varepsilon \approx 15\%$), and $\omega = 19.39°$ ($\varepsilon \approx 25\%$), respectively. Peaks present around the assumed compressed d-spacing with a count number sufficiently greater than the background variation were treated as valid. Bragg spots were observed at $2\theta = 32.53°$ ($\varepsilon = 5.70\%$) at $t = 10$ ps [Fig. 3(b)], at $2\theta = 36.16°$ ($\varepsilon = 17.0\%$) at $t = 16$ ps [Fig. 3(c)], and at $2\theta = 40.80°$ ($\varepsilon = 24.3\%$) at $t = 22$ ps [Fig. 3(d)].

ε and the corresponding d values as a function of t are shown in Fig. 4. The error bars in each plot indicate the FWHM of the peak. The highest ε values in this experiment were 5.70%, 14.9%, and 24.3%, which were measured at $t = 10$, 16, and 22 ps, respectively. The straight line connecting these three points (dashed line in the figure) indicates an increase in the shock wave intensity. It took 12 ps for ε to increase from 5.70% to 24.3%, resulting in an elastic compressive strain rate of 1.55×10^{10}/s. Assuming a linear increase from the onset of the shock initiation, the start of the rise is 6.3 ps after femtosecond laser irradiation, and the 0%–100% rise time is 15.7 ps. The maximum ε at $\omega = 19.39°$ lasted for up to 32 ps, indicating the maximum ε maintained for at least 10 ps.

IV. DISCUSSION

The energy of a femtosecond laser pulse irradiated on a metal is transferred to the electron subsystem in the metal during the

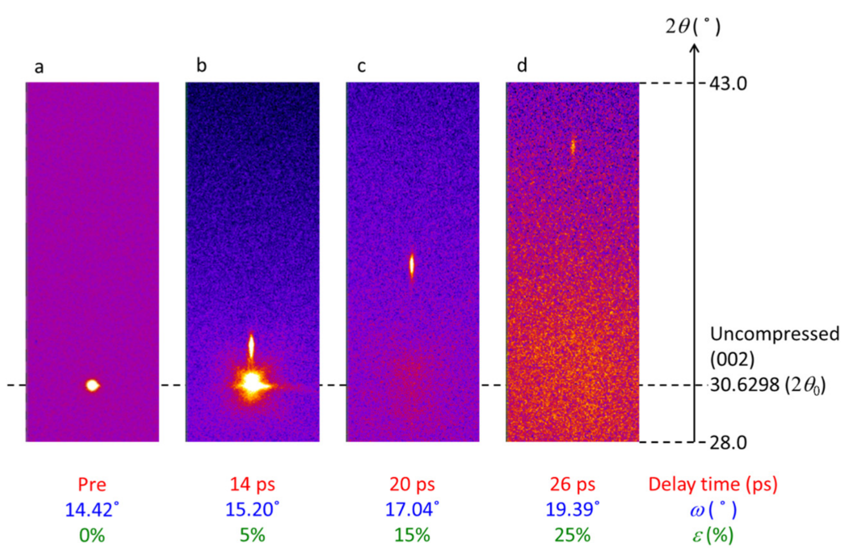

FIG. 2. Typical diffraction patterns recorded at different delay times t and tilt angles ω. The vertical direction in the figure represents the angle in the 2θ direction. (a) Unperturbed pattern recorded before pump laser irradiation. A reflected Bragg spot from the (002) plane of the copper is observed at $2\theta_0 = 30.6298°$. (b) Data acquired at $t = 14$ ps and $\omega = 15.20°$. (c) Data acquired at $t = 20$ ps and $\omega = 17.04°$. (d) Data acquired at $t = 26$ ps and $\omega = 19.39°$. In all cases after femtosecond laser irradiation, Bragg spots are observed at higher angles than in the uncompressed (002) spot.

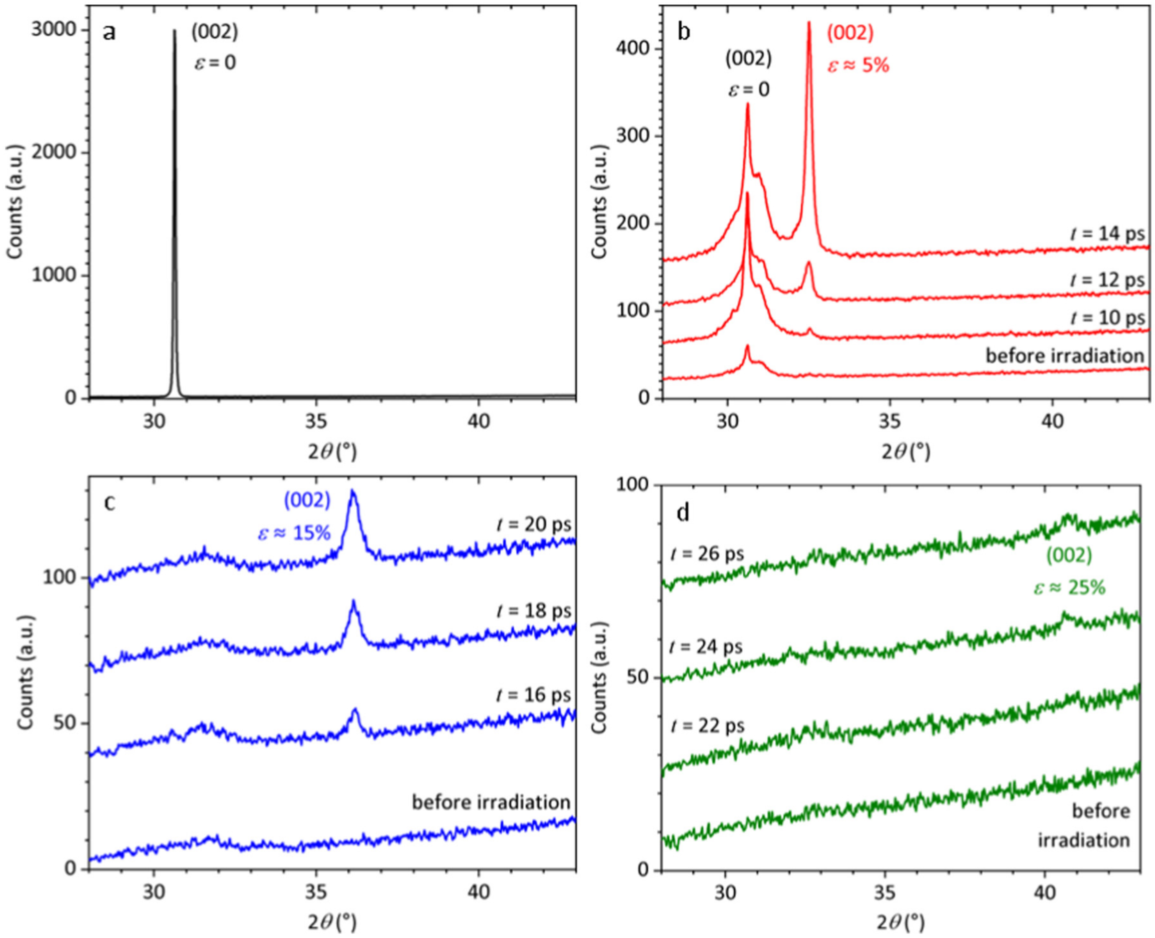

FIG. 3. 1D profiles of XFEL diffraction patterns converted from 3D images. (a) 1D profile in the uncompressed state as shown in Fig. 2(a). (b) 1D profiles at $\omega = 15.20°$, corresponding to $\varepsilon \approx 5\%$, at $t = 10$, 12, and 14 ps. A Bragg spot is visible at $2\theta = 32.53°$, corresponding to $\varepsilon = 5.70\%$ at $t = 10$ ps. (c) 1D profiles at $\omega = 17.04°$, corresponding to $\varepsilon \approx 15\%$, at $t = 16$, 18, and 20 ps. A Bragg spot is visible at $2\theta = 36.16°$, corresponding to $\varepsilon = 17.0\%$ at $t = 16$ ps. (d) 1D profiles at $\omega = 19.39°$, corresponding to $\varepsilon \approx 25\%$, at $t = 22$, 24, and 26 ps. A Bragg spot is visible at $2\theta = 40.80°$ corresponding to $\varepsilon = 24.3\%$ at $t = 22$ ps.

pulse and subsequently from the electron to the lattice subsystem.[42] The relaxation time that transfers energy from the electron subsystem to the lattice subsystem is typically in the order of picoseconds, depending on the material and state.[3,43] Metal ions expand into the atmosphere in the range of tens to hundreds of picoseconds after femtosecond laser irradiation, followed by thermal melting as a secondary thermal effect. Therefore, the shock front observed in this study, which began to rise at 6.3 ps after femtosecond laser irradiation, is driven by the rapid expansion of the lattice subsystem when energy is rapidly transferred from the electron subsystem to the lattice subsystem. This was mentioned in a previous paper,[13] but the experimental results reported here are the first to confirm this by the direct measurement of lattice distortion. The driving mechanism of the shock wave using a laser with a pulse width of sub-nanoseconds or longer is based on the creation of plasma initially during a laser pulse and the subsequent laser pulse heating that plasma. The phenomenon measured in this study is critically different in its driving mechanism from a shock wave driven by such a sub-nanosecond or longer pulse laser.

Sub-nanosecond time-resolved x-ray diffraction (XRD) measurements of the lattice parameters perpendicular and parallel to the shock front in shock-compacted single-crystal copper showed that the shocked copper exhibited hydrostatic compression immediately after uniaxial compression.[44] It has also been reported that copper reaches a shear stress of 18 GPa when shock-compressed by a sub-nanosecond laser at a peak normal elastic stress of 73 GPa and a strain rate of 10^9 /s, followed by a lattice transition from a 1D elastic state to a 3D plastic relaxed state within a few 10 ps.[45] Although the monochromatic x-ray reflection geometry used in this study cannot directly determine the plastic strain in the presence of a large strain gradient in the x-ray penetration region, the elastic strain can be measured with high accuracy. Based on the above interpretation,

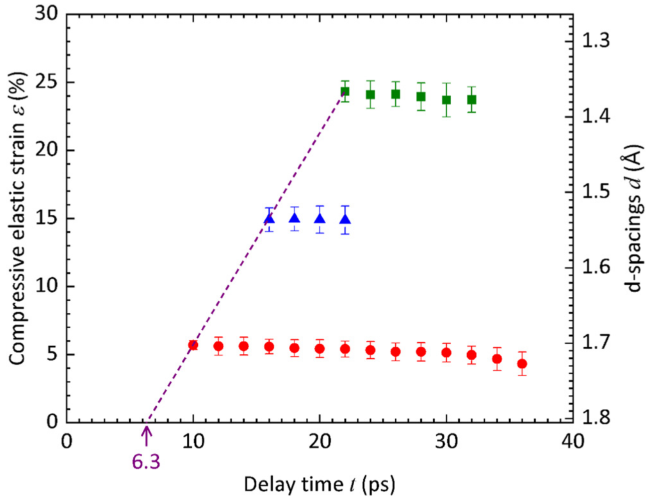

FIG. 4. Compressive elastic strain and the corresponding lattice spacing as a function of delay time. Red circles, blue triangles, and green squares indicate the data measured at $\omega = 15.20°$ ($\varepsilon \approx 5\%$), $\omega = 17.04°$ ($\varepsilon \approx 15\%$), and $\omega = 19.39°$ ($\varepsilon \approx 25\%$), respectively. The error bars in each plot indicate the FWHM of the peak. Assuming a linear rise from the onset of the shock drive, the start of the rise is 6.3 ps after femtosecond laser irradiation, and the 0%–100% rise time is 15.7 ps, corresponding to a strain rate of 1.55×10^{10}/s.

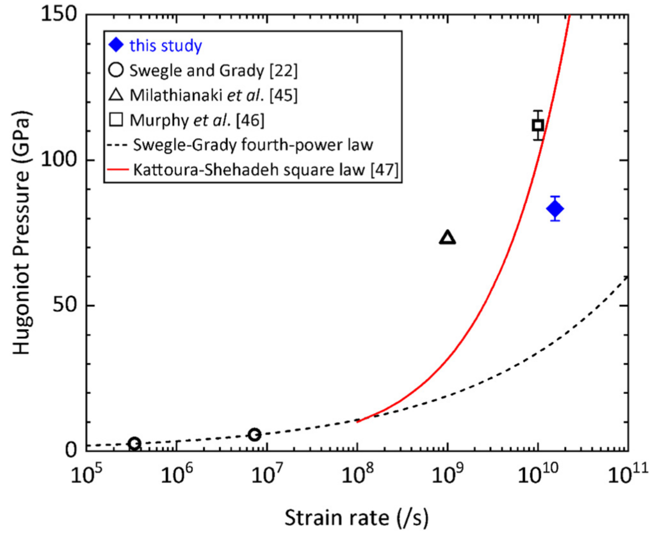

FIG. 5. Relationship between the Hugoniot pressure and strain rate reported in previous studies[22,45–47] and the present study (blue square).

$\varepsilon_x = 24.3\%$ at $t = 22$ ps measured in the present study can be regarded as the strain at the onset of plastic flow, after which the hydrostatic state including plasticity, i.e., the Hugoniot state, can be regarded. The Hugoniot pressure P_H and the shock velocity u_s are expressed as $P_H = c_0^2\varepsilon_H\rho_0/(1 - s\varepsilon_H)^2$ and $u_s = c_0/(1 - s\varepsilon_H)$, respectively, where ε_H is the Hugoniot strain, c_0 is the bulk sound velocity of copper, s is the coefficient that satisfies the relationship between u_s and the particle velocity u_p in the Hugoniot state, and ρ_0 is the initial density of copper. Therefore, we determined the values of $P_H = 83.3$ GPa and $u_s = 6.19$ km/s for $\varepsilon_H = 24.3\%$ using $\rho_0 = 8.93$ g/cm^3, $c_0 = 3.933$ km/s, and $s = 1.500$.[36] The measured rise time is 15.7 ps, indicating that the shock front has a spatial thickness of 97.1 nm.

Theoretically and empirically, it has been shown that the strain rate $\dot{\varepsilon}$ of shock-compressed metals is proportional to the fourth power of P_H (Swegle–Grady fourth power law).[21–23] According to Swegle and Grady, $\dot{\varepsilon} = 7451P_H^4$ for copper.[22] Substituting $\varepsilon \approx = 1.55 \times 10^{10}$/s obtained in this experiment into this relationship yields $P_H = 37.8$ GPa, which is less than the 83.3 GPa estimated using $\varepsilon_H = 24.3\%$ obtained in this study. Figure 5 compares the relationships between P_H and $\dot{\varepsilon}$ obtained in previous studies[21,45,46] with those obtained in the present study. According to multiscale dislocation dynamics simulations for single-crystal copper,[47] up to a strain rate of 10^8/s, the strain rate is proportional to the fourth-power of the Hugoniot pressure based on the existing dislocation multiplication mechanism. However, at higher strain rates, the strain rate is proportional to the square of the Hugoniot pressure based on the dislocation generation mechanism. Because the absolute amounts of normal-direction elastic strain and transverse-direction plastic strain in the shock front are equal under hydrostatic compression, the elastic strain rate of 1.55×10^{10}/s for the shock-rise process obtained in this measurement is equal to the plastic strain rate. Figure 5 shows that the measured data lie between the Swegle–Grady fourth-power law and the square law. This suggests that plasticity begins at the point of maximum elastic compression of the femtosecond laser-driven shock wave and is based on both dislocation multiplication and dislocation generation mechanisms. The unique microstructure observed in the material after femtosecond laser-driven shock compression[9–12] is presumably due to the complicated plastic behavior induced by this extremely large elastic compressive strain rate.

Crowhurst *et al.*[20] reported that shock waves driven by sub-nanosecond laser pulses in aluminum deposited on glass reached a peak pressure of 43 GPa at strain rates exceeding 10^{10}/s and followed the Swegle–Grady fourth power law.[21–23] Despite similar strain rates, our results differ from those reported by Crowhurst *et al.*[20] as they do not follow the Swegle–Grady fourth power law. This difference could be due to the variations in the material properties of the copper used in this study and the aluminum used by Crowhurst *et al.*,[20] such as the viscosity and dislocation behavior, laser characteristics such as the pulse width and wavelength used to drive the shock, and the laser irradiation environment (open surface vs interface). Investigating these factors would be an interesting topic for future research. If the strain is uniform in the x-ray penetration depth region, information regarding the elastic strain corresponding to the Bragg peak position in XRD can be obtained, along with the plastic strain corresponding to the peak width.[14] However, in the case of femtosecond laser-driven shock waves with a large spatial strain gradient of over 100 nm, as shown in this study, the peak width includes both plastic and spatial elastic gradient components; thus, the plastic strain cannot be directly discussed from the present measurement results. The combination of *in situ* investigations, such as spatially macroscopic and temporally ultrafast pump–probe measurements[15–17] and molecular dynamics simulations[29,48,49] with post-process investigations, such as residual microstructure analysis[8–12,49] could further enhance our understanding of the unique phenomena induced by femtosecond laser-driven shock waves.

V. CONCLUSIONS

In summary, the elastic strain during the femtosecond laser-driven shock rise in copper was directly measured using XFEL diffraction. The (002) plane, which is nearly parallel to the sample surface, took 12 ps to reach a compressive elastic strain of 24.3%, which increased linearly from 5.70%, corresponding to a compressive elastic strain rate of 1.55×10^{10}/s. Assuming a linear increase from the onset of the shock wave, the 0%–100% rise time of the shock wave was 15.7 ps. Based on the fact that plasticity begins as soon as the shock wave elastically rises and the material enters the Hugoniot state, the Hugoniot pressure and shock velocity are estimated to be 83.3 GPa and 6.19 km/s, respectively, at a compressive strain of 24.3%, where the shock front has a spatial thickness of 97.1 nm. The relationship between the strain rate measured in this experiment and the estimated Hugoniot pressure lies between the Swegle–Grady fourth power law and the square law, suggesting that the plasticity initiated by femtosecond laser-driven shock waves at the most elastically compressed state is due to both dislocation multiplication and generation mechanisms.

ACKNOWLEDGMENTS

The authors thank M. Yoshida, T. Nakayama, R. Takekuma, Y. Mori, S. Inoue, Y. Komatsubara, N. Asaoka, A. Higuchi, S. Fujisawa, M. Hotta, Y. Takami, R. Mitsuoka, Y. Tanaka, Y. Nagai, T. Fukui, and the engineering staff of SACLA for their experimental support. The XFEL experiments were performed at the BL3 of SACLA under the approval of the Japan Synchrotron Radiation Research Institute (JASRI) (Proposal Nos. 2021B8031, 2022A8031, and 2023B8023). This study was supported, in part, by MEXT Quantum Leap Flagship Program (MEXT Q-LEAP) (Grant No. JPMXS0118068348) and JSPS KAKENHI (Grant Nos. 19K22061, 20H02048, 23K17702, and 24K21579). The Amada Foundation, The Light Metal Educational Foundation, Inc., Osawa Scientific Studies Grants Foundation, Mazak Foundation, and Suzuki Foundation.

AUTHOR DECLARATIONS

Conflict of Interest

The authors have no conflicts to disclose.

Author Contributions

Naoya Egashira: Formal analysis (equal); Investigation (equal); Methodology (equal); Writing – original draft (equal). **Tomoki Matsuda:** Investigation (equal); Methodology (equal); Writing – review & editing (equal). **Takuo Okuchi:** Funding acquisition (supporting); Investigation (equal); Methodology (equal); Writing – review & editing (equal). **Yusuke Seto:** Formal analysis (equal); Investigation (equal); Methodology (equal); Software (lead). **Yusuke Ito:** Investigation (equal); Methodology (equal). **Takahisa Shobu:** Investigation (equal); Methodology (equal). **Nobuhiko Nakanii:** Conceptualization (supporting); Formal analysis (equal); Investigation (equal); Methodology (equal); Writing – review & editing (equal). **Yuichi Inubushi:** Investigation (equal); Methodology (equal); Writing – review & editing (equal). **Tadashi Togashi:** Investigation (equal); Methodology (equal). **Kohei Miyanishi:** Investigation (equal); Methodology (equal). **Tsutomu Mashimo:** Investigation (equal); Writing – review & editing (equal). **Tomokazu Sano:** Conceptualization (lead); Data curation (lead); Formal analysis (equal); Funding acquisition (lead); Investigation (equal); Methodology (equal); Project administration (lead); Supervision (lead); Writing – original draft (equal); Writing – review & editing (lead).

DATA AVAILABILITY

The data that support the findings of this study are available from the corresponding author upon reasonable request.

REFERENCES

[1]D. Strickland and G. Mourou, Opt. Commun. **56**, 219–221 (1985).
[2]T. Sano, T. Eimura, R. Kashiwabara, T. Matsuda, Y. Isshiki, A. Hirose, S. Tsutsumi, K. Arakawa, T. Hashimoto, K. Masaki, and Y. Sano, J. Laser Appl. **29**, 012005 (2017).
[3]B. N. Chichkov, C. Momma, S. Nolte, F. von Alvensleben, and A. Tünnermann, Appl. Phys. A **63**, 109–115 (1996).
[4]T. Kawashima, T. Sano, A. Hirose, S. Tsutsumi, K. Masaki, K. Arakawa, and H. Hori, J. Mater. Process. Technol. **262**, 111–122 (2018).
[5]U. Trdan, T. Sano, D. Klobčar, Y. Sano, J. Grum, and R. Šturm, Corros. Sci. **143**, 46–55 (2018).
[6]M. Yoshida, I. Nishibata, T. Matsuda, Y. Ito, N. Sugita, A. Shiro, T. Shobu, K. Arakawa, A. Hirose, and T. Sano, J. Appl. Phys. **132**, 075101 (2022).
[7]T. Sano, H. Mori, E. Ohmura, and I. Miyamoto, Appl. Phys. Lett. **83**, 3498–3500 (2003).
[8]S. Juodkazis, K. Nishimura, S. Tanaka, H. Misawa, E. G. Gamaly, B. Luther-Davies, L. Hallo, P. Nicolai, and V. T. Tikhonchuk, Phys. Rev. Lett. **96**, 166101 (2006).
[9]A. Vailionis, E. G. Gamaly, V. Mizeikis, W. Yang, A. V. Rode, and S. Juodkazis, Nat. Commun. **2**, 445 (2011).
[10]M. Tsujino, T. Sano, O. Sakata, N. Ozaki, S. Kimura, S. Takeda, M. Okoshi, N. Inoue, R. Kodama, K. F. Kobayashi, and A. Hirose, J. Appl. Phys. **110**, 126103 (2011).
[11]T. Matsuda, T. Sano, K. Arakawa, and A. Hirose, Appl. Phys. Lett. **105**, 021902 (2014).
[12]T. Matsuda, T. Sano, K. Arakawa, and A. Hirose, J. Appl. Phys. **116**, 183506 (2014).
[13]R. Evans, A. D. Badger, F. Falliès, M. Mahdieh, T. A. Hall, P. Audebert, J.-P. Geindre, J.-C. Gauthier, A. Mysyrowicz, G. Grillon, and A. Antonetti, Phys. Rev. Lett. **77**, 3359–3362 (1996).
[14]T. Sano, T. Matsuda, A. Hirose, M. Ohata, T. Terai, T. Kakeshita, Y. Inubushi, T. Sato, K. Miyanishi, M. Yabashi, T. Togashi, K. Tono, O. Sakata, Y. Tange, K. Arakawa, Y. Ito, T. Okuchi, T. Sato, T. Sekine, T. Mashimo, N. Nakanii, Y. Seto, M. Shigeta, T. Shobu, Y. Sano, T. Hosokai, T. Matsuoka, T. Yabuuchi, K. A. Tanaka, N. Ozaki, and R. Kodama, Sci. Rep. **13**, 13796 (2023).
[15]D. S. Moore, S. D. McGrane, and D. J. Funk, "Ultra-short laser shock dynamics," in *Shock Wave Science and Technology Reference Library*, edited by Y. Horie (Springer-Verlag, 2007), Vol. 2, pp. 47–104.

[16]D. S. Moore, J. Opt. Soc. Am. B **35**, B1–B15 (2018).
[17]M. S. Powell, P. R. Bowlan, S. F. Son, C. A. Bolme, K. E. Brown, D. S. Moore, and S. D. McGrane, Rev. Sci. Instrum. **90**, 063001 (2019).
[18]K. T. Gahagan, D. S. Moore, D. J. Funk, R. L. Rabie, S. J. Buelow, and J. W. Nicholson, Phys. Rev. Lett. **85**, 3205–3208 (2000).
[19]S. I. Ashitkov, M. B. Agranat, G. I. Kanel', P. S. Komarov, and V. E. Fortov, JETP Lett. **92**, 516–520 (2010).
[20]J. C. Crowhurst, M. R. Armstrong, K. B. Knight, J. M. Zaug, and E. M. Behymer, Phys. Rev. Lett. **107**, 144302 (2011).
[21]D. E. Grady, Appl. Phys. Lett. **38**, 825–826 (1981).
[22]J. W. Swegle and D. E. Grady, J. Appl. Phys. **58**, 692–701 (1985).
[23]D. E. Grady, J. Appl. Phys. **107**, 013506 (2010).
[24]V. Schmidt, W. Husinsky, and G. Betz, Phys. Rev. Lett. **85**, 3516–3519 (2000).
[25]E. G. Gamaly, A. V. Rode, B. Luther-Davies, and V. T. Tikhonchuk, Phys. Plasmas **9**, 949–957 (2002).
[26]S. Amoruso, R. Bruzzese, M. Vitiello, N. N. Nedialkov, and P. A. Atanasov, J. Appl. Phys. **98**, 044907 (2005).
[27]H. Dachraoui and W. Husinsky, Appl. Phys. Lett. **89**, 104102 (2006).
[28]V. V. Zhakhovskii and N. A. Inogamov, JETP Lett. **92**, 521–526 (2010).
[29]V. V. Zhakhovsky, M. M. Budzevich, N. A. Inogamov, I. I. Oleynik, and C. T. White, Phys. Rev. Lett. **107**, 135502 (2011).
[30]V. H. Whitley, S. D. McGrane, D. E. Eakins, C. A. Bolme, D. S. Moore, and J. F. Bingert, J. Appl. Phys. **109**, 013505 (2011).
[31]M. A. Meyers, F. Gregori, B. K. Kad, M. S. Schneider, D. H. Kalantar, B. A. Remington, G. Ravichandran, T. Boehly, and J. S. Wark, Acta Mater. **51**, 1211 (2003).
[32]A. Schropp, R. Hoppe, V. Meier, J. Patommel, F. Seiboth, Y. Ping, D. G. Hicks, M. A. Beckwith, G. W. Collins, A. Higginbotham, J. S. Wark, H. J. Lee, B. Nagler, E. C. Galtier, B. Arnold, U. Zastrau, J. B. Hastings, and C. G. Schroer, Sci. Rep. **5**, 11089 (2015).
[33]F. Barbato, S. Atzeni, D. Batani, D. Bleiner, G. Boutoux, C. Brabetz, P. Bradford, D. Mancelli, P. Neumayer, A. Schiavi, J. Trela, L. Volpe, G. Zeraouli, N. Woolsey, and L. Antonelli, Sci. Rep. **9**, 18805 (2019).
[34]L. Antonelli, F. Barbato, D. Mancelli, J. Trela, G. Zeraouli, G. Boutoux, P. Neumayer, S. Atzeni, A. Schiavi, L. Volpe, V. Bagnoud, C. Brabetz, B. Zielbauer, P. Bradford, N. Woolsey, B. Borm, and D. Batani, Europhys. Lett. **125**, 35002 (2019).
[35]T. Ishikawa *et al.*, Nat. Photonics **6**, 540–544 (2012).
[36]O. E. Jones and J. D. Mote, J. Appl. Phys. **40**, 4920–4928 (1969).
[37]A. C. Mitchell and W. J. Nellis, J. Appl. Phys. **52**, 3363–3374 (1981).
[38]R. Chau, J. Stölken, P. Asoka-Kumar, M. Kumar, and N. C. Holmes, J. Appl. Phys. **107**, 023506 (2010).
[39]Y. Inubushi, K. Tono, T. Togashi, T. Sato, T. Hatsui, T. Kameshima, K. Togawa, T. Hara, T. Tanaka, H. Tanaka, T. Ishikawa, and M. Yabashi, Phys. Rev. Lett. **109**, 144801 (2012).
[40]Y. Seto and M. Ohtsuka, J. Appl. Crystallogr. **55**, 397 (2022).
[41]Y. Seto (2025). "IPAnalyzer" software, Github repository. See https://github.com/seto77/IPanalyzer/ for the software, which performs image analysis on 2D diffraction patterns acquired with imaging plates and CCD/CMOS cameras and converts them into 1D X-ray diffraction profiles. The installation file and documentation on how to use the software are also available at the GitHub page.
[42]S. I. Anisimov, B. L. Kapeliovich, and T. L. Perel'man, Sov. Phys. JETP **39**, 375 (1974).
[43]N. Medvedev and I. Milov, Phys. Rev. B **102**, 064302 (2020).
[44]A. Loveridge-Smith, A. Allen, J. Belak, T. Boehly, A. Hauer, B. Holian, D. Kalantar, G. Kyrala, R. W. Lee, P. Lomdahl, M. A. Meyers, D. Paisley, S. Pollaine, B. Remington, D. C. Swift, S. Weber, and J. S. Wark, Phys. Rev. Lett. **86**, 2349–2352 (2001).
[45]D. Milathianaki, S. Boutet, G. J. Williams, A. Higginbotham, D. Ratner, A. E. Gleason, M. Messerschmidt, M. M. Seibert, D. C. Swift, P. Hering, J. Robinson, W. E. White, and J. S. Wark, Science **342**, 220–223 (2013).
[46]W. J. Murphy, A. Higginbotham, G. Kimminau, B. Barbrel, E. M. Bringa, J. Hawreliak, R. Kodama, M. Koenig, W. McBarron, M. A. Meyers, B. Nagler, N. Ozaki, N. Park, B. Remington, S. Rothman, S. M. Vinko, T. Whitcher, and J. S. Wark, J. Phys.: Condens. Matter **22**, 065404 (2010).
[47]M. Kattoura and M. A. Shehadeh, Philos. Mag. Lett. **94**, 415–423 (2014).
[48]B. J. Demaske, V. V. Zhakhovsky, N. A. Inogamov, and I. I. Oleynik, Phys. Rev. B **87**, 054109 (2013).
[49]V. Zhakhovsky, Y. Kolobov, S. Ashitkov, N. Inogamov, I. Nelasov, S. Manokhin, V. Khokhlov, D. Ilnitsky, Y. Petrov, A. Ovchinnikov, O. Chefonov, and D. Sitnikov, Phys. Fluids **35**, 096104 (2023).